Novel core-shell bioceramic silica-Berberis vulgaris: synthesis and characterization

Mahmood F. Chawshli*, Shakhawan K. Hamad

Conservative Department, Hawler Medical University, Erbil 44000, Iraq

ARTICLE INFO

ABSTRACT

Enhancements in bioceramic mixtures represent a significant avenue for achieving superior mechanical and biological properties. Therefore, the present study aimed to extract active compounds from Berberis vulgaris stems and fruits collected from the Khorasan province, employing advanced analytical techniques such as GC-MS and FTIR to elucidate the composition of these extracts. The derived extracts were utilized to synthesize novel nanocomposites, denoted as SiO_2-MPS-stem extract and SiO_2-MPS-fruit extract. Comprehensive characterization of these composites was conducted through SEM, EDX mapping, FTIR, and XRD analyses. The characterization measurements validated the successful coating of silica with the extracts, resulting in a core-shell nanostructure with particle sizes below 60 nm. These composites were incorporated into bioceramics for dental root fillings with an equal weight ratio. The bioceramic material was subjected to the same aforementioned characterization techniques, revealing that their sizes fell within the nanoscale range, not exceeding 70 nanometers. The results indicated a core-shell configuration for the nanomaterials, with the shell comprising the bioceramic component of bioceramic-SiO_2-MPS-fruit extract and bioceramic-SiO_2-MPS-stem extract.

Introduction

The root canal treatment procedure involves using endodontic files to widen the root canal and applying chemical disinfectants to cleanse the area. The process aims to eliminate any remaining living or dead tissues, eradicate the microbes residing in the root canal system, disrupt any microbial biofilm, and eliminate any accumulated hard debris resulting from the root canal instrumentation. After that, packing and sealing the canal with a suitable sealing material to achieve a fluid-tight seal space in the channel (1).

Endodontics is an evolving field driven by continuously introducing new technologies and techniques. The significant growth in endodontics is mainly attributable to advancements in endodontic material sciences. One recent groundbreaking material that has transformed endodontics is the introduction of bio-ceramic root canal obturation sealers (2).

Calcium silicate-based bio-ceramic endodontic sealers (Portland Cement) have many remarkable properties for good prognosis of the endodontic treatment; their resemblance to biological hydroxyapatite gives them outstanding biocompatibility properties. They also possess intrinsic osteoinductive capabilities that enable them to absorb osteoinductive substances in cases where bone healing occurs nearby. In addition, they serve as a regenerative scaffold of resorbable lattices that offer a framework for tissue rebuilding, which eventually dissolves as the body undergoes tissue regeneration (3). The eradication of bacteria from the root canal involves chemical disinfection and mechanical Preparation of the canal system. However, eliminating microbes from the canal system is unachievable despite the available chemical irrigation and automated strategies. Therefore, using root canal-filling materials that possess antibacterial properties is advantageous. Calcium silicate-based bio-ceramic endodontic sealers have excellent antibacterial properties; bacterial sequestration occurs due to precipitation in situ after setting, resulting in antibacterial properties, especially against Enterococcus faecalis (4). Due to the increasing resistance of pathogenic bacteria to antibiotics and chemotherapeutic agents, researchers are increasingly focused on exploring alternative products and treatment options for oral diseases.

Consequently, natural phytochemicals extracted from plants and traditionally used in medicine are emerging as viable replacements for synthetic chemicals (5). Berberis vulgaris member of the Berberidaceae family thrives across Asia and Europe. The B. vulgaris is a 1–3 m tall shrub with prickly yellow bark and oblique leaves, followed by yellow blooms and round red berries. This plant's roots, bark, leaves, stem, and fruit have all been used for medicinal purposes. This plant's primary alkaloids are berberine, berberine, and palmitine. Its principal constituents provide diverse antibacterial effects (6).

Another attempt to enhance the endodontic sealing material is the incorporation of nanomaterials into the endodontic sealing materials; nanotechnology refers to the investigation of biology, technology, and architecture at microscopic scales, typically ranging from 1 to 100 nanometers. Its applications span various sectors and involve manipulating the size and structure of nanoparticles at a scale of one billionth of a meter. In simpler terms, nanotechnology involves creating functional entities that are 100 nanometers or smaller in size (7). The utilization of plants for the synthesis of nanoparticles (NPs) is an ad-

---

vanced chemical technique that offers numerous advantages in terms of profitability and environmental sustainability. The green synthesis of metal and metal-oxide NPs is a fascinating area within nanoscience, and plants have emerged as the most promising candidates for large-scale applications in this field, especially silica nanoparticles that enhance the mechanical and physical properties of chemical compounds (8).

Materials and Methods

The materials used in this study were obtained from Sigma-Aldrich. The Berberis vulgaris stems and fruits were collected and processed in-house. Analytical grade solvents and reagents were employed for extraction and synthesis processes; the following materials were used:
1. Berberis vulgaris stems: Fresh stems of Berberis vulgaris were collected and carefully selected for the extraction of active compounds.
2. Berberis vulgaris fruits: Fresh fruits of Berberis vulgaris were collected and prepared for the extraction of active compounds.
3. Solvents: Analytical grade solvents (deionized water, methanol, cyclohexane) were obtained to extract the active compounds from the Berberis vulgaris stems and fruits and to prepare the nanocomposites.
4. γ-methacryloxypropyltrimethoxysilane (MPS) was utilized for the functionalization of the silica.
5. Bioceramic sealer was purchased from south korea.

Instrumentations
1. Gas Chromatography-Mass Spectrometry (GC-MS): Agilent 7890B Gas Chromatograph coupled with Agilent 5977A Mass Spectrometer.
2. Fourier Transform Infrared Spectroscopy (FTIR): Shimadzu 8400 SSpectrum.
3. Scanning Electron Microscopy (SEM): ZEISS Field Emission Scanning Electron Microscope or FEI Quanta FEG 250 Scanning Electron Microscope.
4. Energy-Dispersive X-ray Spectroscopy (EDX): Oxford Instruments X-MaxN Energy-Dispersive X-ray Spectrometer or Bruker XFlash X-ray Detector.
5. X-ray diffraction (XRD): Shimadzu XRD-6000 X-ray Diffractometer.

Berberis extraction procedure
To extract the medicinal compounds from the Berberis plant, the stems and fruits were processed separately using a series of steps.

Firstly, the plant parts were carefully placed in a shaded area to dry out completely. Once dried, the plant parts were finely ground into a powder using a blender.

In detail, the powdered plant material was mixed with 70% ethyl alcohol, maintaining a ratio of 1 part plant powder (36.2935g) to 7 parts alcohol (254 ml). The mixture was left to stir at 750 rpm at boiling temperature for 48 hours in the Clevenger apparatus, allowing the alcohol to extract the desired compounds effectively.

Following the extraction period, the resulting mixture underwent filtration twice using Whatman No. 4. Subsequently, the extracts were centrifuged at -4 °C for 10 minutes at 11745 rpm to separate any remaining impurities.

To eliminate any residual traces of ethanol and water, specific measures were taken. The extracts were placed in an incubator packed with calcium chloride for ten days at a controlled temperature of 37 °C to evaporate the ethanol content; lastly, the extracts obtained from different parts of the Berberis plant were subjected to sterilization using 0.22 μm micropore filters, ensuring the removal of any potential contaminants (9).

Silanization of silica nanoparticles
In this experimental procedure, a synthesis route for obtaining 3-methacryloxypropyltrimethoxysilane- (γ-MPS-) silanized SiO_2 nanoparticles were employed. Initially, a mixture comprising 5.0 g of SiO_2 nanopowder, 0.1 g of n-propylamine, and 0.6 g of γ-MPS was introduced into a beaker containing 100 mL of cyclohexane. The components were subjected to ultrasound (probe 6, 150 Watt) for 2 minutes, and then the mixture was stirred at room temperature for 30 minutes to ensure thorough dispersion. Subsequently, the suspension underwent continuous stirring for an additional 30 minutes while the temperature was maintained at 65 °C—this controlled thermal treatment aimed to promote the reaction kinetics and enhance the desired functionalization process. Following the reaction period, the solvent was removed utilizing a rotary evaporator set at 65 °C, facilitating the evaporation process. The resulting precipitates were then subjected to a series of washing steps, using absolute ethanol as the washing agent. This rigorous washing procedure was performed three times to eliminate any residual unreacted γ-MPS and ensure the purity of the obtained functionalized nanoparticles. To finalize the synthesis, the washed powders were subjected to vacuum drying at 80 °C for 24 hours. This drying step aimed to remove any remaining solvent and facilitate the formation of a dry, stable product suitable for subsequent Characterization and analysis (10).

## Synthesis and characterization of berberis extract–silica nanoparticle
The Silanization of berberis stem or berberis fruit extract was carried out using the batch method. The loading ratio employed was m(SiO_2):m(berberis)= 10:1. To summarize the procedure, SiO_2 and berberis extracts were dissolved in a solution of polyethylene glycol-400 (1% in distilled water) and stirred for 24 hours at 30 °C. Subsequently, the solution underwent centrifugation (SSU-173) at 12000 rpm for ten minutes. The resulting material, loaded with the berberis extract, was then subjected to repeated washing with distilled water and subsequently dried at a temperature of 50 °C overnight, yielding the final product: SiO_2-MPS-Fruit extract and SiO_2-MPS-Stem extract nanocomposites.

Preparation of the dental sealer composites
The specific amounts of SiO_2-MPS extracts (1%, 2%, and 3%) were carefully measured and combined with the bioceramic sealer paste. Subsequently, the mixture underwent a rigorous agitation process, employing a magnetic stirrer and a mechanical stirrer (dental stone laboratory engine) for 20 minutes. This dual agitation method ensured comprehensive mixing and dispersion of the SiO_2-MPS extracts within the bioceramic sealer paste, promoting even distribution of the constituents. The combined action of these stirring techniques facilitated the formation of a uniform mixture, thereby ensuring optimal integration of

Table 1. XRD data and crystalline size of SiO_2 derivative.

No.	Pos. [°2θ]	d-spacing [Å]	FWHM [°2θ]	Crystallite Size only [nm]	
			SiO_2		
1	21.7877	4.07587	0.8659	10.6	Mean (10.7)
2	33.4031	2.68036	0.8659	10.8	
			MPS		
1	22.5749	4.30488	0.9190	9.21	
			Fruit-MPS		
1	21.6334	4.39820	0.9283	9.10	
			Stem-MPS		
1	22.5974	4.31000	0.9001	9.40	

Scheme 1. Synthesis step of the bioceramic composites.
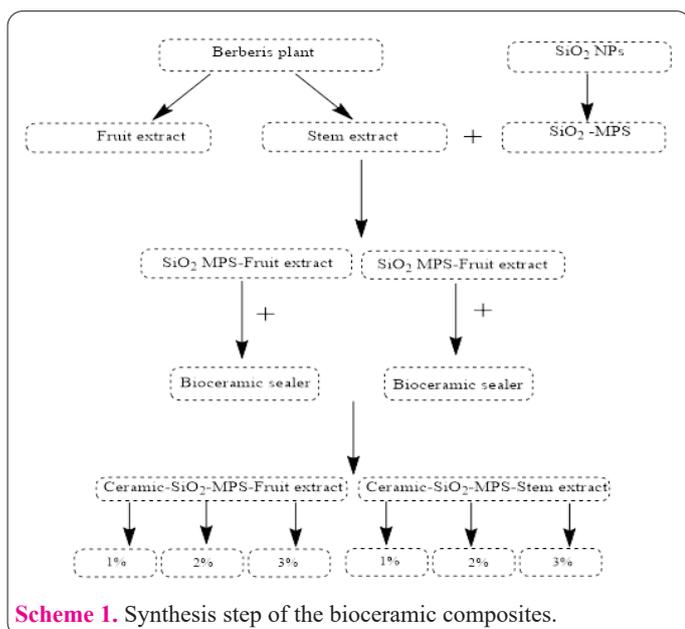
the SiO_2-MPS extracts with the bioceramic sealer paste, as illustrated in the scheme (1).

Results

Characterization of SiO_2 nanoparticles and its nanocomposite

SiO_2 nanoparticles

FTIR

In the case of silica nanoparticles, the FTIR spectrum (Figure S1 and Table S1) can provide insight into the chemical composition and structure of the material. The prominent peaks observed in the FTIR spectrum of silica nanoparticles are:

1.   The band at 3410 cm⁻¹ is due to the stretching vibration of the hydroxyl (–OH) group, which is typically present on the surface of silica nanoparticles.

2.   The band at 1654 cm⁻¹ is due to the bending vibration of the –OH group, which is also present on the surface of the nanoparticles.

3.   The band at 1095 cm⁻¹ is due to the stretching vibration of the Si–O–Si bond (asymmetrical), a characteristic silica feature.

4.   The band at 956 cm⁻¹ is due to the stretching vibration of the Si–O–H bond, which is also present on the surface of the nanoparticles.

5.   The band at 806 cm⁻¹ is due to the bending vibra-

tion of the Si–O–Si bond (symmetrical), which is another characteristic feature of silica.

6.   The band at 470 cm⁻¹ is due to the bending vibration of the Si–O–Si bond (asymmetrical).

The presence of these bands is an indication of the existence of silica in its pure amorphous form (11, 12, 13).

XRD

Silica nanoparticles exhibit broad XRD peaks due to their small size, resulting in decreased diffraction intensity and peak broadening. The peaks observed in the XRD pattern of the provided silica nanoparticles occur at approximately 21.8° and 33.4° (2θ). These correspond to the (101) and (200) crystal planes of hexagonal silica, respectively (14, 15). The d-spacing for these peaks is 4.08 Å and 2.68 Å, respectively. The full width at half maximum (FWHM) of the peaks indicates the degree of crystallinity, which in this case is 0.87°2θ for both peaks. See (Figure 1 and Table 1).

SEM and EDX of SiO_2 nanoparticles

The SEM characterization of the silica nanoparticles in (Figure 2 and Table 2) shows that the particles have a spherical morphology and are well-dispersed in the sample.

Table 2. SEM data of silica nanoparticles.

Characteristic	Observations
Morphology	Spherical
Particle Size Range	15.55-29.34 nm
Particle Dispersion	Well-dispersed

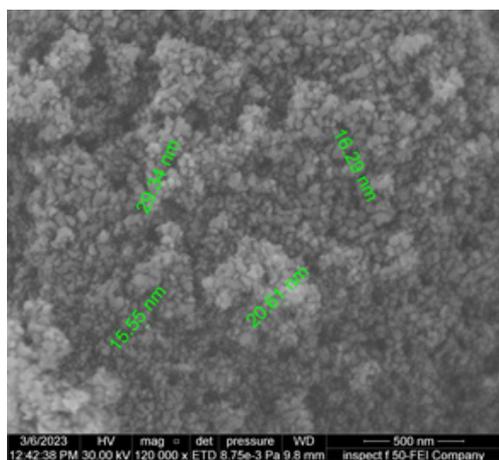**Figure 1.** XRD of SiO_2 NPs.
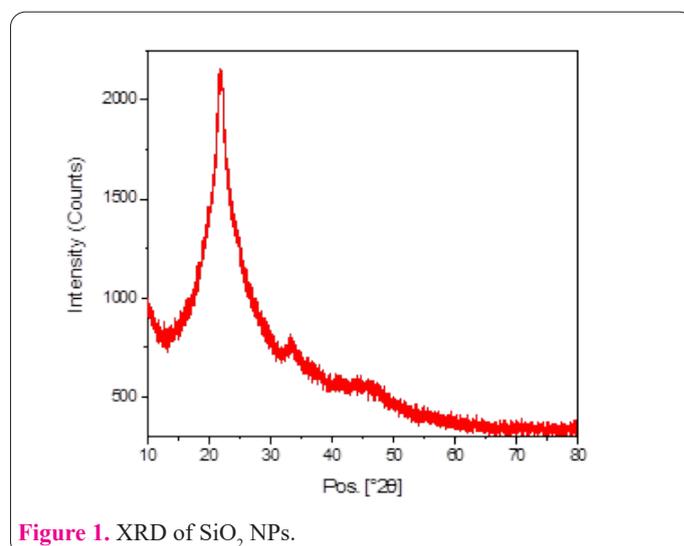
Figure 2. SEM of SiO$_2$ nanoparticles.

The average particle sizes are 15.55-29.34 nm, indicating that the model contains a range of particle sizes. (16, 17).

The EDX analysis of the silica nanoparticles in (Figure S2) shows two peaks of Si and O at 1.74 and 0.52 keV. Furthermore, the EDX offers that the particles are composed mainly of oxygen (50.5 wt%) and silicon (49.5 wt%). This elemental composition is consistent with the design of silica (O, 53.26; Si, 46.74), which has a chemical formula of SiO$_2$. The well-dispersed nature of the nanoparticles is also observed in the EDX mapping, which shows a homogeneous distribution of oxygen and silicon across the sample. The EDX analysis provides essential information about the elemental composition of the nanoparticles.

MPS nanoparticles

FTIR

The FTIR spectrum of SiO2 functionalized with 3-methacryloxypropyltrimethoxysilane reveals characteristic bands as illustrated in (Figure S3 and Table S2). The band at 3433 cm-1 indicates hydroxyl (-OH) groups on the nanoparticle surface, implying hydrophilicity and potential interaction with polar molecules. The band at 2954 cm-1 represents the methylene (-CH2-) groups of the coupling agent, confirming successful attachment. The band at 1720 cm-1 corresponds to the carbonyl (C=O) group, verifying the presence of the coupling agent. The band at 1630 cm-1 confirms the methacrylate functional group. Bands at 1459 cm-1, 1435 cm-1, 1099 cm-1, 798 cm-1, and 470 cm-1 provide further evidence of the SiO2 core in the functionalized nanoparticles (18, 19).

XRD

The XRD pattern of the silanized silica nanoparticles (Figure 3) shows one prominent peak at approximately 22.6° (2θ). This peak corresponds to the (101) plane of the hexagonal crystal structure of silica, with a d-spacing of 4.30 Å. The peak's full width at half maximum (FWHM) is 0.92°2θ, indicating that the silanized silica nanoparticles are relatively amorphous with some degree of crystallinity. The crystallite size can be estimated using the Scherrer equation, which relates the FWHM to the crystallite size. Based on the FWHM and assuming a spherical crystallite shape, the crystallite size is estimated at 9.21 nm. This value suggests that the silanized silica nanoparticles have a relatively small crystallite size, consistent with the small particle size of silica nanoparticles. It should be noted that

the XRD pattern provided only shows one peak, which indicates that the silanized silica nanoparticles are not highly crystalline. This could be due to the modification of the surface properties of the nanoparticles through Silanization, which may have disrupted the crystal structure of the nanoparticles (19).

SEM and EDX of mesoporous silica nanoparticles

The SEM analysis indicates that after functionalizing with 3-methacryloxypropyltrimethoxysilane, the particle size range increased to 17-36.43 nm, with some changes in the structure. This change in size and layout is likely due to the addition of the functional group, which can lead to aggregation or rearrangement of the nanoparticles. However, the particles still maintain a spherical shape and are well dispersed, indicating that the functionalization process did not significantly affect the overall morphology or dispersion of the nanoparticles. See (Figure 4 and Table 3).

The EDX analysis in (Figure S4) indicates that the SiO$_2$ nanoparticles have been successfully functionalized with 3-methacryloxypropyltrimethoxysilane, as evidenced by the presence of carbon (C) in addition to the expected silicon (Si) and oxygen (O) elements. The weight
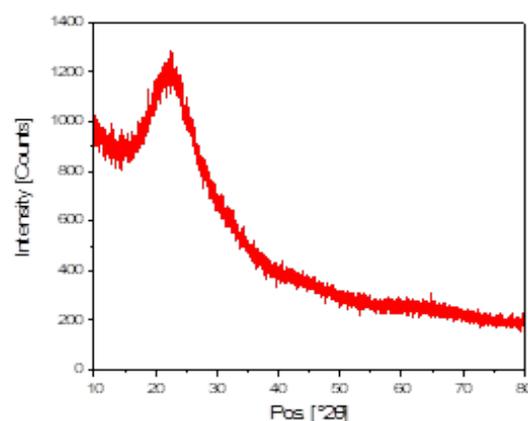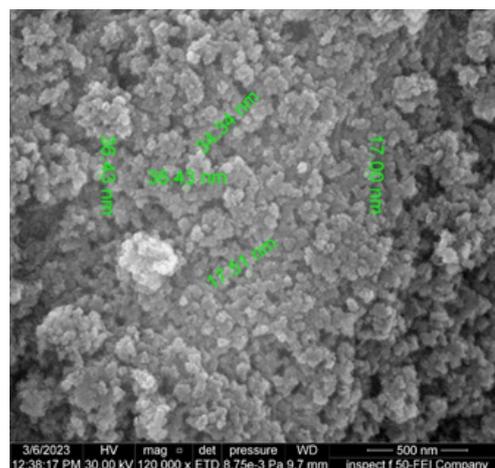

Figure 3. XRD of MPS NPs.

Figure 4. SEM of MPS nanoparticles.

Table 3. SEM data with SiO$_2$-3-methacryloxypropyltrimethoxysilane.

Characteristic	Observations
Morphology	Spherical
Particle Size Range	17-36.43 nm
Particle Dispersion	Well-dispersed

percentages of each component are 19.3% for C, 48.1% for O, and 32.6% for Si. The presence of C suggests that the functionalization process was successful and that the 3-methacryloxypropyltrimethoxysilane molecules have been covalently bonded to the surface of the SiO_2 nanoparticles. The weight percentage of Si is slightly lower than that of the unfunctionalized SiO_2 due to the presence of a carbon skeleton in the structure. Overall, the EDX analysis confirms the successful functionalization of SiO_2 nanoparticles with 3-methacryloxypropyltrimethoxysilane (19).

STEM extract@SiO₂ MPS nanoparticles

FTIR

A. FTIR of STEM

The FTIR spectrum of the extracted organic molecules from the plant stem reveals absorption bands at various wavenumbers seen in (Figure S5 and Table S3). 2-Methoxy-4-vinylphenol is identified from bands at 1600 cm-1 (C=C stretching) and 3410 cm-1 (exocyclic O-H stretching). Ethyl phthalate is identified from bands at 1639 cm-1 and 1620 cm-1 (C=O stretching). 1-(N)-hydroxyethyl-9-phenyl-4,5,6,7-tetrahydro[1]benzothieno[2,3-c]pyridine is identified from the band at 1458 cm-1 (phenyl group deformation). Decanedioic acid, bis(2-ethylhexyl) ester is identified from the band at 1770 cm-1 (C=O stretching). Octasiloxane,1,1,3,3,5,5,7,7,9,9,11,11,13,13,15,15-hexadecamethyl is identified from bands 779 cm-1 (Si-O-Si rocking) and 470 cm-1 (Si-O-Si bending). 2-Undecanone, 6,10-dimethyl is identified from the band at 1072 cm-1 (C=O stretching). The bands at 2927 cm-1 and 1377 cm-1 are attributed to aliphatic C-H stretching and bending vibrations (20, 21).

B. FTIR of STEM extract@SiO₂ MPS nanoparticles

The FTIR spectrum of SiO_2-3-methacryloxypropyltrimethoxysilane-stem extract in (Figure S6 and Table S4) shows several characteristic peaks attributed to different functional groups present in the sample. The broad peak at 3425 cm-1 is due to the O-H stretching vibration of hydroxyl groups in the organic molecules present in the extract. The peak at 2954 cm-1 corresponds to the C-H stretching vibration of the methylene groups in the organic molecules. The peak at 2897 cm-1 is due to the C-H stretching vibration of the methyl groups in the 3-methacryloxypropyltrimethoxysilane molecule. The peak at 1720 cm-1 is due to the C=O stretching vibration of the ester group in the 3-methacryloxypropyltrimethoxysilane molecule. The peak at 1635 cm-1 is attributed to the C=C stretching vibration of the vinyl group in the 3-methacryloxypropyltrimethoxysilane molecule. The peak at 1465 cm-1 is due to the deformation vibration of the CH_2 group in the methylene chain of the 3-methacryloxypropyltrimethoxysilane molecule. The peak at 1435 cm-1 is due to the deformation vibration of the CH_3 group in the 3-methacryloxypropyltrimethoxysilane molecule. The peak at 1408 cm-1 is attributed to the Si-O-C stretching vibration in the 3-methacryloxypropyltrimethoxysilane molecule.

The peak at 1300 cm-1 is due to the C-N stretching vibration of the nitrogen-containing organic molecule 1-(N)-hydroxyethyl-9-phenyl-4,5,6,7-tetrahydro[1]benzothieno[2,3-c]pyridine present in the stem extract.

The peak at 1168 cm-1 is due to the C-O stretching vibration of the ester group in ethyl phthalate.

The peak at 1099 cm-1 is attributed to the Si-O stretching vibration in the SiO_2-3-methacryloxypropyltrimethoxysilane hybrid material. The peak at 937 cm-1 corresponds to the C-H deformation vibration of the methylene groups in the organic molecules. The peak at 813 cm-1 is due to the C-S stretching vibration in the 1-(N)-hydroxyethyl-9-phenyl-4,5,6,7-tetrahydro[1]benzothieno[2,3-c]pyridine molecule. The peak at 794 cm-1 corresponds to the deformation vibration of the Si-O-C bond in the SiO_2-3-methacryloxypropyltrimethoxysilane hybrid material. The 690 cm-1 and 651 cm-1 peaks are attributed to the Si-O-Si bond's bending vibration in the SiO_2-3-methacryloxypropyltrimethoxysilane hybrid material. Finally, the peak at 470 cm-1 corresponds to the Si-O-Si stretching vibration in the SiO_2-3-methacryloxypropyltrimethoxysilane mixed material (22).

XRD of STEM extract-SiO₂ MPS nanoparticles

The XRD pattern of SiO_2-3-methacryloxypropyltrimethoxysilane-stem (Figure 5) extract shows a diffraction peak at 2θ value of 22.5974°, corresponding to a d-spacing of 4.31000Å. The peak's FWHM (full width at half maximum) is 0.900°2θ, and the crystallite size is 9.10 nm (19). Comparing the two XRD patterns of SiO_2-3-methacryloxypropyltrimethoxysilane and SiO_2-3-methacryloxypropyltrimethoxysilane-stem extract, we can see that both samples have similar crystallite sizes, but there is a slight difference in the position and width of their diffraction peaks. This could be due to the difference in the crystal structure of the two samples, which may be attributed to the stem extract in the SiO_2-3-methacryloxypropyltrimethoxysilane-stem.

SEM of MPS-stem extract nanoparticles

The SEM analysis of SiO_2-3-methacryloxypropyltrimethoxysilane-stem extract (Figure 6 and Table 4) shows an average particle size range of 24.4-37.15 nm, which is
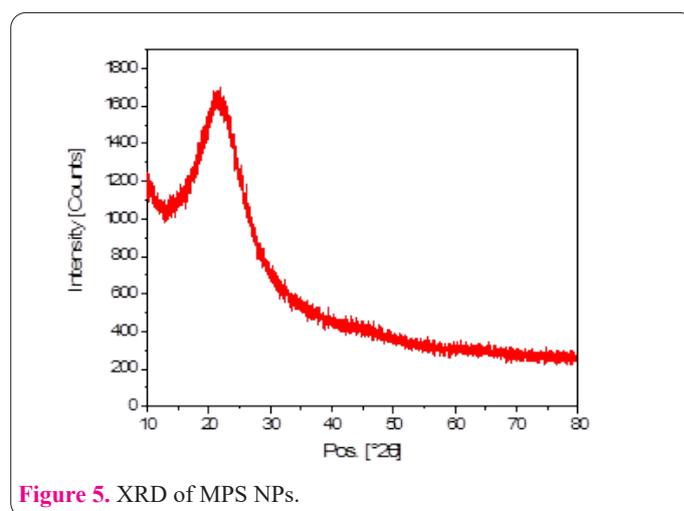

Figure 5. XRD of MPS NPs.

Table 4. SEM data of SiO_2-3-methacryloxypropyltrimethoxysilane-stem extract.

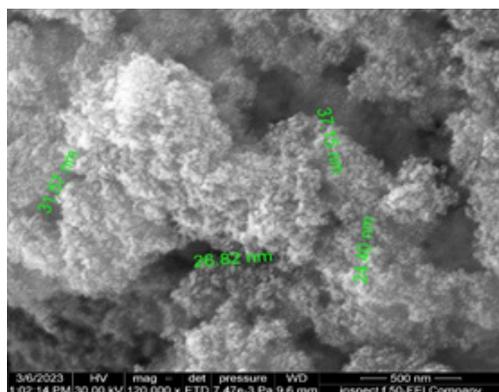| Characteristic	Observations
Average Particle Size Range	24.4-37.15 nm
Particle Shape	Spherical shape
Dispersion	Well dispersed

Figure 6. SEM of MPS-stem extract nanoparticles.

slightly larger than the particle size range of SiO_2-3-methacryloxypropyltrimethoxysilane (17-36.43 nm). Adding the stem extract has contributed to the increase in particle size, possibly due to agglomeration or clustering of the nanoparticles. However, the particles still maintain a spherical shape and are well dispersed, indicating that the stem extract did not significantly affect the overall morphology or dispersion of the nanoparticles. Overall, SEM analysis provides valuable information on nanoparticles' morphology and size distribution, which can help determine their suitability for various applications such as drug delivery, catalysis, and sensing.

The EDX analysis of SiO_2-3-methacryloxypropyltrimethoxysilane-stem extract (Figure S7) shows the presence of carbon (C), nitrogen (N), silicon (Si), and oxygen (O) elements. The weight percentages of each component are 19.0% for C, 4.2% for N, 47.8% for O, and 29.0% for Si.

Compared to the EDX analysis of SiO_2-3-methacryloxypropyltrimethoxysilane, the weight percentage of carbon in SiO_2-3-methacryloxypropyltrimethoxysilane-stem extract is slightly lower (19.0% vs. 19.3%), indicating that the functionalization process was successful in both cases the proof of the functionalization was the complete appearance of the organic content in the EDX. The weight percentage of silicon in SiO_2-3-methacryloxypropyltrimethoxysilane-stem extract is slightly higher (29.0% vs. 32.6%) compared to SiO_2-3-methacryloxypropyltrimethoxysilane, which may be due to the addition of stem extract. The presence of nitrogen in SiO_2-3-methacryloxypropyltrimethoxysilane-stem extract indicates the presence of the stem extract, which is not present in SiO_2-3-methacryloxypropyltrimethoxysilane.

Overall, the EDX analysis confirms the successful functionalization of SiO_2 nanoparticles with 3-methacryloxypropyltrimethoxysilane and the successful addition of stem extract to form SiO_2-3-methacryloxypropyltrimethoxysilane-stem extract.

FRUIT extract@SiO_2 MPS nanoparticles

FTIR

A. FTIR of Fruit
Based on the FTIR spectrum (FigureS8 and Table S5), the identified functional groups are as follows:
5,4'-Dimethoxy-2-methylbibenzyl: C-H stretching (2931 cm-1), aromatic ring (1624 cm-1), C-H bending (1404 cm-1), C-O bond (1076 cm-1), 4,7,7-Trimethylbi-

cyclo[3.3.0]octan-2-one: Carbonyl group (1728 cm-1), C-H stretching (2931 cm-1), C-O bond (1076 cm-1), Urea N,N'-dibutyl-N,N'-dimethyl: N-H stretching (3329 cm-1), C-N stretching (1624 cm-1), C-N bending (1404 cm-1), C-H stretching (2931 cm-1), carbonyl (C=O) stretching (1728 cm-1). Diethyl Phthalate: Carbonyl (C=O) stretching (1728 cm-1), C-O bending (1269 cm-1, 1145 cm-1).

Linoleic acid: C-H stretching (2921 cm-1), carbonyl (C=O) stretching (1728 cm-1), C=C bond (1624 cm-1), CH2 bending (1404 cm-1) (23).

B. FTIR of FRUIT extract@SiO_2 MPS nanoparticles
The FTIR spectrum of SiO_2-3-methacryloxypropyltrimethoxysilane-fruit extract see (Figure S9 and Table S6) reveals critical absorption bands: O-H stretching (3479 cm-1), C=O stretching (1720 cm-1), C=C stretching (1635 cm-1), Si-O-C stretching (1103 cm-1), and Si-O-Si bending (466 cm-1). These bands confirm the presence of hydroxyl, carbonyl, double bonds, and siloxane bonds, indicating successful synthesis (24).

XRD of FRUIT extract@SiO_2 MPS nanoparticles

The XRD analysis of SiO2-methacryloxypropyltrimethoxysilane-fruit extract in (Figure 7) provided the following information: Peak position: 21.6334°2θInterplanar spacing: 4.39820°2θ Full width at half maximum (FWHM): 0.9283Estimated crystallite size: 9.10 nm Comparison with SiO2-methacryloxypropyltrimethoxysilane revealed a slight shift in peak position and d-spacing for SiO2-methacryloxypropyltrimethoxysilane-fruit extract. However, the FWHM values were comparable, indicating similar crystallinity. The estimated crystallite size was slightly smaller in the fruit extract composite. These differences suggest that the presence of the fruit extract may have influenced the crystallinity and particle size of the composite material.

SEM and EDX of MPS-fruit extract nanoparticles

SEM (Scanning Electron Microscopy) analysis of SiO_2-methacryloxypropyltrimethoxysilane-fruit extract in (Figure 8 and Table 5) revealed a particle size range of 22.39-34.00 nm. Comparing this with the precursor material SiO_2-methacryloxypropyltrimethoxysilane, which exhibited an average particle size range of 17-36.43 nm, we can observe that the particle sizes in the fruit extract are similar. Furthermore, this is larger than the crystallite size estimated from the XRD pattern, which was 9.10 nm. It is not uncommon for there to be differences in particle
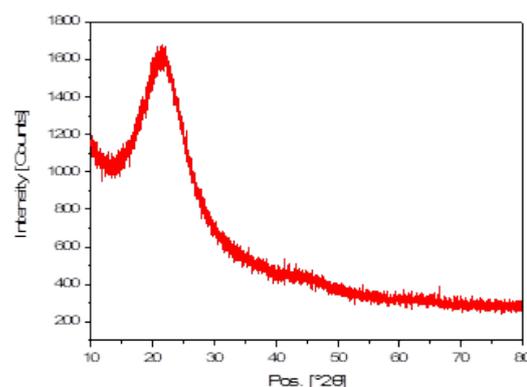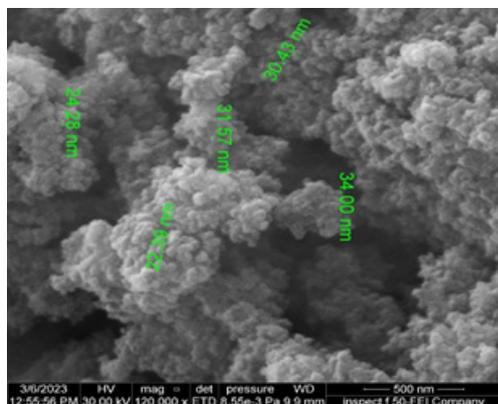

Figure 7. XRD of Fruit-MPS NPs.

Table 5. SEM data of SiO$_2$-3-methacryloxypropyltrimethoxysilane-fruit extract.

Characteristic	Observations
Average Particle Size Range	22.39-34.00 nm
Particle Shape	Irregular spherical shape
Dispersion	Well dispersed

Figure 8. SEM of MPS-fruit extract nanoparticles.

size estimates between XRD and SEM techniques due to differences in the measurement methods and assumptions used. However, the SEM results indicate that the particles in SiO$_2$-methacryloxypropyltrimethoxysilane-fruit extract are relatively small and uniform, which is desirable for many applications.

The EDX analysis of SiO2-3-methacryloxypropyltrimethoxysilane-fruit extract in (Figure S10) revealed the presence of carbon (C), nitrogen (N), silicon (Si), and oxygen (O) elements. The weight percentages of these elements are as follows: 19.5% for C, 4.4% for N, 48.0% for O, and 28.0% for Si. C and Si indicate the successful functionalization of SiO2 nanoparticles with 3-methacryloxypropyltrimethoxysilane, as is seen in the supplementary document. The weight percentage of Si is slightly lower than that of unfunctionalized SiO2, which is expected. The presence of N suggests the adsorption of nitrogen-containing compounds from the fruit extract onto the nanoparticle surface during synthesis.

Characterization of ceramic nanoparticles and their nanocomposites

Characterization of bioceramic

The components of bioceramic sealer are ZrO$_2$ nanoparticles: Zirconia (ZrO$_2$) nanoparticles, as mentioned earlier, are ceramic materials known for their biocompatibility and mechanical properties. Zirconia nanoparticles can contribute to the overall strength and stability of the sealer.

Calcium silicate: Calcium silicate compounds have bioactive and sealing properties, such as tricalcium silicate (Ca3SiO5) or dicalcium silicate (Ca2SiO4). As mentioned, calcium silicate can absorb moisture from the surrounding tissues to form Calcium Aluminate Hydrate (CAH) gel and Calcium Silicate Hydrate (CSH) gel, which aid in sealing the root canal.

Aluminum silicate: Aluminum silicate, a compound containing aluminum and silicon, may have specific functions within the formulation of the sealer. Its precise role may vary depending on the manufacturer's design, and it can contribute to the sealer's physical or chemical properties.

Ca(OH)$_2$ (Calcium hydroxide): Calcium hydroxide is a well-known dental material with antimicrobial and bioactive properties. Its presence in the sealer formulation suggests it may contribute to the antimicrobial activity and biocompatibility of META biomed Ceraseal (3).

FTIR

The FTIR spectrum of the ceramic material in (Figure S11 and Table S7) reveals characteristic bands: O-H stretching (3383 cm-1), C-H stretching (2924 cm-1 and 2877 cm-1), C=O stretching (1654 cm-1), aromatic C=C stretching (1577 cm-1), CH3 deformation (1473 cm-1), C-H bending (1350 cm-1), Si-OH stretching (1103 cm-1), Zr-OH stretching (1064 cm-1), Si-O stretching (945 cm-1), Si-O-Ca or Si-O-Al bending (528 cm-1), and Zr-O bending (420 cm-1). These bands indicate the presence of hydroxyl, organic compounds, silicate, and zirconium-based species in the ceramic material (25).

XRD

Based on the given composition of Zirconia (ZrO$_2$), calcium silicate, aluminum silicate, and calcium hydroxide, the XRD peaks can be characterized as follows:

1. 28.68°: This peak could be attributed to calcium silicate or Ca(OH)$_2$ in the mixture.
2. 30.66°, 35.50, 41.71°, 50.72°, 60.29°, 63.22°, and 74.34°: This peak may be related to the crystalline phase of Zirconia (ZrO$_2$) in the mixture, which corresponds to the phases 101, 002, 102, 200, 211, 202 and 220, respectively (26).
3. 32.02° and 33°: presence of unknown component.
4. 34.84°: This peak corresponds to a crystallographic phase associated with calcium silicate (27). See (Figure 9 and Table 6).

SEM and EDX

The SEM characterization of the bioceramic sealer in (Figure 10 and Table 7) shows that the particles have an irregular morphology and are well-dispersed in the sample. The average particle sizes are 60-120 nm, indicating that the sample contains a range of particle sizes. Furthermore, this suggests that the particles are relatively small, and their size distribution may be relatively narrow. It is worth

Table 6. XRD data of bioceramic.

Pos. [°2Th.]	FWHM [°2Th.]	Particle size [nm]	Average particle size [nm]
28.6818	0.2460	34.84	
30.6687	0.2952	29.17	
32.0217	0.1968	43.90	29.39
32.6546	0.2460	35.17	
34.8426	0.1968	44.22	
35.5045	0.3444	25.32	
41.7180	0.7872	11.29	
50.7236	0.3444	26.68	
60.2961	0.6888	13.94	
63.2272	0.4920	19.82	
74.3434	1.2000	8.68	
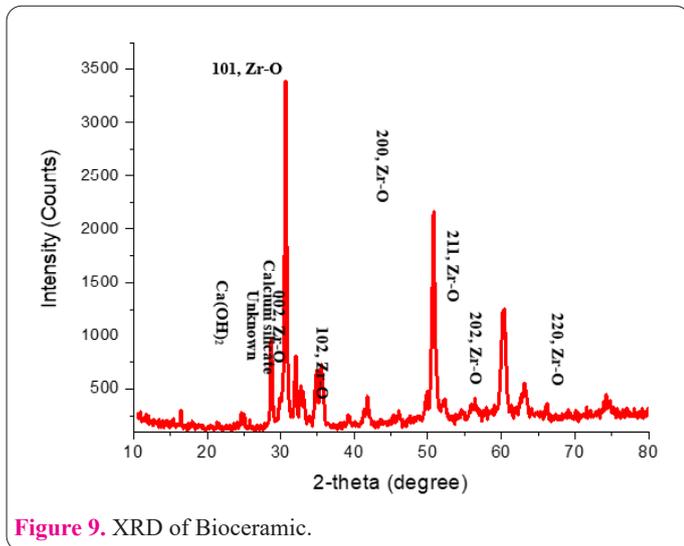
Figure 9. XRD of Bioceramic.
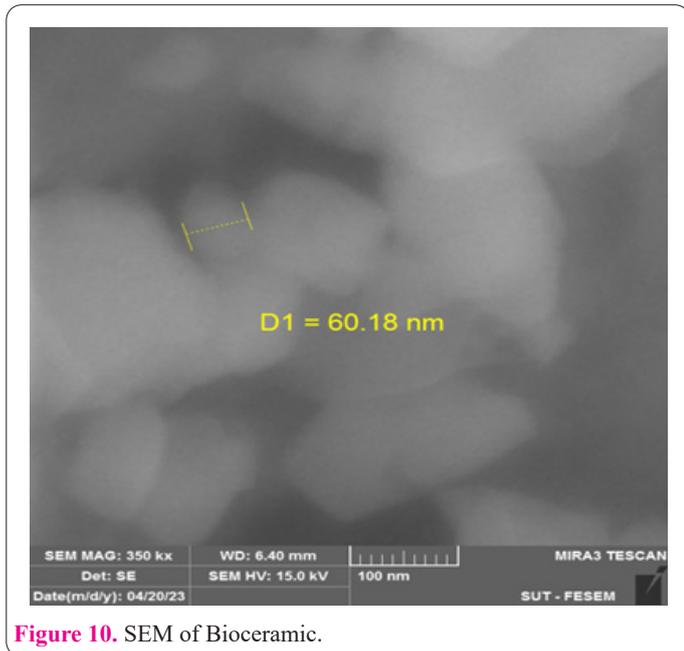
Figure 10. SEM of Bioceramic.

Table 7. SEM data of bioceramic.

Characteristic	Observations
Morphology	irregular
Particle Size Range	60-120 nm
Particle Dispersion	Well-dispersed

noting that these particles may be present due to zirconia.

Based on the given weight percentages in (Figure S12), the composition and positions of the elements in the bioceramic sample can be determined. The bioceramic contains zirconium (40.9%) in the form of zirconium dioxide ($ZrO2$), which is known for its high hardness and biocompatibility. Oxygen (25.7%) is present in various compounds, including $ZrO2$, calcium hydroxide ($Ca(OH)_2$), aluminum silicate, and calcium silicate. Calcium (16.6%) is found in $Ca(OH)2$ and calcium silicate, both commonly used in bioceramics for bone regeneration. Carbon (8.6%) suggests including an organic component, likely from binders or additives. Silicon (3.2%) is present in aluminum and calcium silicate, critical parts of silicate-based materials. Aluminum (0.7%) is found in aluminum silicate, providing desirable properties in ceramics. The peak positions for each element in X-ray fluorescence spectroscopy indicate typical values, such as Zr (2.04 keV), O (0.53 keV), Ca (3.69 keV), C (0.28 keV), Si (1.74 keV), and Al (1.49 keV). While other elements may be present but not accurately detected, the measurements show that zirconium is the most abundant element, followed by Calcium, silicon, and aluminum. The ingredients are evenly distributed throughout the composition, as shown in the map.

Ceramic-SiO$_2$-MPS-Fruit extract

FTIR of ceramic-SiO$_2$-MPS-Fruit extract

The FTIR spectrum of the ceramic-SiO2-MPS-Fruit extract in (Figure S13 and Table S8) exhibits characteristic bands: O-H stretching (3394 cm-1), C-H stretching (2904 cm-1 and 2873 cm-1), C=O stretching (1716 cm-1), C=C stretching (1577 cm-1 and 1654 cm-1), CH3 deformation (1477 cm-1), C-H bending (1350 cm-1), Si-OH stretching (1099 cm-1), Zr-OH stretching (1099 cm-1), Si-O stretching (945 cm-1), Si-O-Ca or Si-O-Al bending (590 cm-1), and Zr-O bending (420 cm-1). These bands indicate the presence of hydroxyl, organic compounds, carbonyl groups, aromatic compounds, methyl groups, alkane groups, silanol groups, silicate groups, zirconium hydroxide, and zirconium oxide in the material, reflecting its complex composition resulting from the combination of ceramic and SiO$_2$-MPS-Fruit extract (24).

XRD of ceramic-SiO$_2$-MPS-Fruit extract

Based on the given composition of zirconia (ZrO_2), calcium silicate, aluminum silicate, and calcium hydroxide, the XRD peaks can be characterized as follows:

1. 21.35 with FWHM 1.03595: This peak attributed to the amorphous phase of SiO$_2$-MPS-Fruit extract

2. 28.80°: This peak could be attributed to calcium silicate or $Ca(OH)_2$ in the mixture.

3. 30.65°, 35.55, 41.83°, 50.69, 60.21°, 63.05° and 74.747: This peak may be related to the crystalline phase of Zirconia (ZrO_2) in the mixture, which corresponds to the phases 101, 002, 102, 200, 211, 202 and 220, respectively.

4. 31.97°: an unknown component that could be a thickening agent.

34.85°: This peak corresponds to a crystallographic phase associated with calcium silicate. See Figure 11 and Table 8.

Table 8. XRD data of ceramic-SiO$_2$-MPS-Fruit extract.

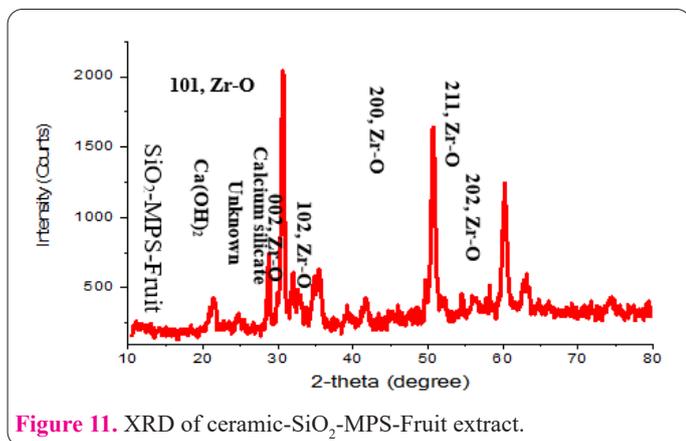| Pos. [°2Th.]	FWHM [°2Th.]	Particle size [nm]	Average Particle size [nm]
21.3500	1.03595	8.16	
28.8034	0.3444	24.89	
30.6513	0.3936	21.87	
31.9758	0.3936	21.95	
34.8553	0.3000	29.01	
35.5528	0.3936	22.15	19.68
41.8304	0.3936	22.58	
50.6994	0.3444	26.68	
60.2138	0.4920	19.51	
63.0571	0.7872	12.38	
74.4752	1.4400	7.24	

Figure 11. XRD of ceramic-SiO_2-MPS-Fruit extract.

SEM and EDX of ceramic-SiO_2-MPS-Fruit extract

The prepared ceramic-SiO_2-MPS-fruit extract composite material exhibited regular nanosphere morphology. This indicates that the particles in the composite possessed a more spherical and uniform shape than the irregular ceramic particles. Additionally, the particle size range of the composite material was reduced to 23-46 nm, indicating a decrease in particle size when compared to the original ceramic particles. This size reduction could be attributed to including SiO_2, MPS, and fruit extract in the composite. Moreover, the particle dispersion in the composite material was described as well-dispersed, suggesting an excellent distribution of particles throughout the composite without any significant clustering or agglomeration. See (Figure 12 and Table 9).

The EDX analysis of the ceramic-SiO_2-MPS-Fruit extract composite (Figure S14) provided the following elemental composition: Based on the EDX results, it can be observed that Zr (Zirconium) is present in the composite, accounting for 17.67% of the total weight. This suggests that Zr is a constituent element of the composite material.

Table 9. SEM data of ceramic-SiO_2-MPS-Fruit extract.

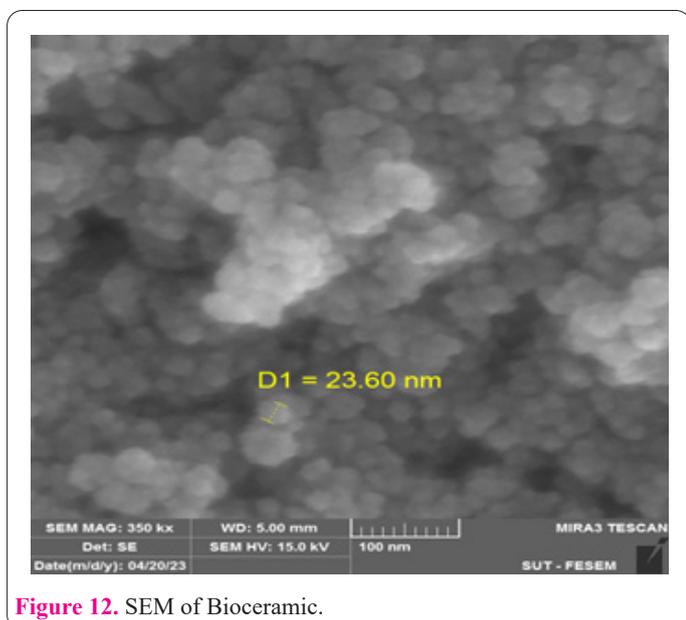| Characteristic	Observations
Morphology	Regular sphere like
Particle Size Range	23-46 nm
Particle Dispersion	Very well-dispersed

Figure 12. SEM of Bioceramic.

Furthermore, the EDX analysis implies that Zr is predominantly located on the surface of the composite. The decrease in Zr weight percentage in the composite compared to the bioceramic (40.9) is likely influenced by the addition of SiO_2-MPS-Fruit extract. The SiO_2-MPS and Fruit extract components may have displaced or substituted some of the Zr atoms on the surface, resulting in a lower weight percentage of Zr. This can occur due to the different chemical interactions and bonding characteristics between Zr and the other components of the composite.

Furthermore, the increase in carbon content observed in the ceramic-SiO_2-MPS-Fruit extract composite compared to the original ceramic material is likely attributed to adding the Fruit extract component.

Ceramic-SiO_2-MPS-Stem extract

FTIR of ceramic-SiO_2-MPS-Stem extract

The FTIR spectrum of the ceramic-SiO2-MPS-Stem extract in (Figure S15 and Table S8)reveals characteristic bands indicating the presence of various functional groups and compounds. These include hydroxyl groups (3371 cm-1), C-H and C=O groups in organic compounds (2924 cm-1, 2877 cm-1, 1716 cm-1), vinyl and aromatic groups (1639 cm-1, 1581 cm-1), alkane groups (1469 cm-1, 1354 cm-1), silicate groups (1296 cm-1, 941 cm-1), silanol and zirconium hydroxide groups (1103 cm-1, 1064 cm-1), zirconium oxide (420 cm-1), and specific bonds in the hybrid materials (Si-O-Ca/Al, Si-O-Si). The analysis suggests a complex composition resulting from the combination of ceramic, SiO2-MPS-Stem extract, and specific organic molecules used in the Preparation (21).

XRD of ceramic-SiO_2-MPS-Stem extract

Based on the given composition of zirconia (ZrO_2), calcium silicate, aluminum silicate, and calcium hydroxide, the XRD peaks can be characterized as follows:
1. 20.77 with FWHM 0.919: This peak is attributed to the amorphous phase of SiO_2-MPS-Stem extract.
2. 28.69°: This peak could be attributed to calcium silicate or $Ca(OH)_2$ in the mixture.
3. 30.54°, 35.47, 41.67°, 50.17, 60.15°, 63.11°, and 74.74°: This peak may be related to the crystalline phase of Zirconia (ZrO_2) in the mixture, which corresponds to the phases 101, 002, 102, 200, 211, 202 and 220, respectively.
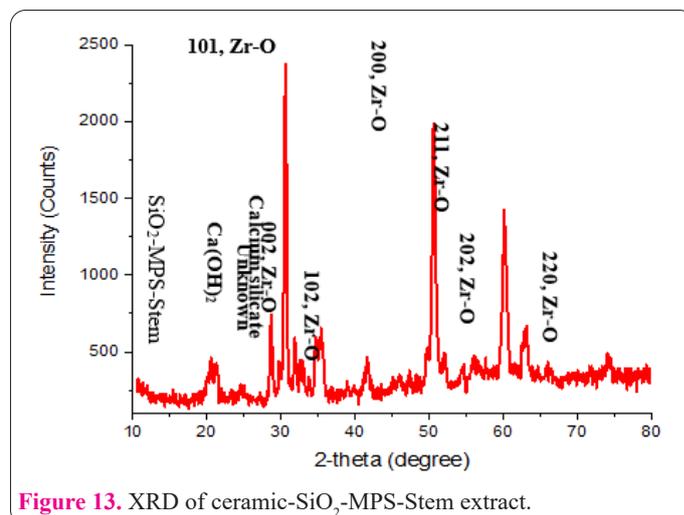4. 31.87° and 33°: an unknown component that could be

Figure 13. XRD of ceramic-SiO_2-MPS-Stem extract.

Table 10. XRD data of ceramic-SiO$_2$-MPS-Stem extract.

Pos. [°2Th.]	FWHM [°2Th.]	Particle size [nm]	Average particle size [nm]
20.77	0.919	9.19	
28.6913	0.2952	29.03	
30.5411	0.3444	24.99	
31.8712	0.2460	35.10	
34.6744	0.2952	29.47	
35.4745	0.4920	17.72	
41.6712	0.3936	22.57	24.30
50.6035	0.2460	37.34	
60.1572	0.4920	19.50	
63.1103	0.6000	16.24	
74.7301	0.3999	26.13	

a thickening agent.

34.67°: This peak corresponds to a crystallographic phase associated with calcium silicate. See (Figure 13 and Table 10).

SEM and EDX of ceramic-SiO$_2$-MPS-Stem extract

The SEM analysis of the ceramic material revealed an irregular morphology with particles ranging in size between 60 and 120 nm. These ceramic particles were well-dispersed without significant agglomeration because of the shape of the nanoparticles. However, after incorporating SiO2-MPS-Stem extract into the composite material, the particle morphology changed to quasi-regular nanospheres. This indicated a more uniform and spherical shape than the irregular ceramic particles. See (Figure 14 and Table 11).

Based on the EDX results, it can be observed that Zr (Zirconium) is present in the composite with 19.2% of the total weight. This suggests that Zr is a constituent element of the composite material. Furthermore, the EDX analysis implies that Zr is predominantly located as the core of the composite, not as in the case of the composite containing fruit extract. Regarding the decrease in Zr weight percentage in the composite compared to the ceramic (40.9), it is likely influenced by the addition of SiO$_2$-MPS-Stem extract. In summary, the EDX analysis confirmed the presence of Zr in the ceramic-SiO$_2$-MPS-Stem extract composite, with a higher concentration on the surface. The decrease in Zr weight percentage may be attributed to incorporating SiO$_2$-MPS-Stem extract, which can influence the distribution and interaction of Zr atoms in the composite (See Figure S16).

Discussion

Nanotechnology, manipulating matter at the nanoscale, has emerged as a promising field with diverse applications in various sectors, including dentistry. The integration of nanotechnology into dental practices has the potential to revolutionize diagnosis, treatment, and preventive care (14). This discussion essay explores the applications of nanotechnology in dentistry, highlighting its impact on oral health and patient care.

In the current study, Fourier transforms infrared (FTIR) spectroscopy was used, a powerful analytical technique widely used to identify and quantify chemical compounds

Table 11. SEM data of ceramic-SiO$_2$-MPS-Stem extract.

Characteristic	Observations
Morphology	quasi-regular nanospheres
Particle Size Range	40-89 nm
Particle Dispersion	well-dispersed
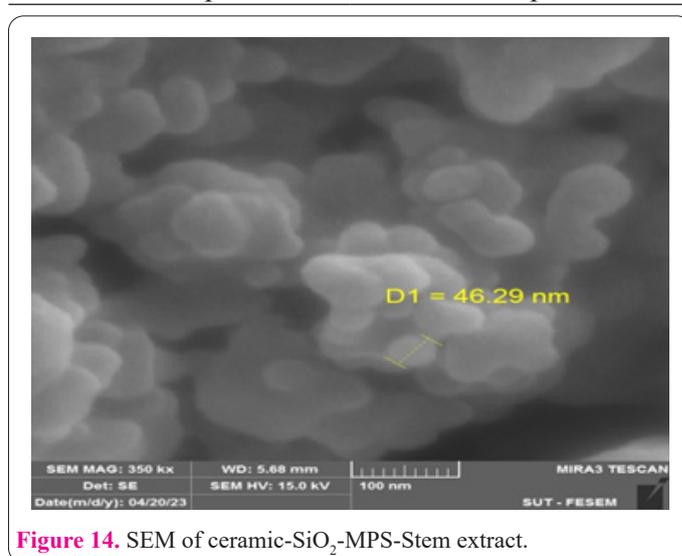
Figure 14. SEM of ceramic-SiO$_2$-MPS-Stem extract.

in a sample. It works by measuring the absorption or transmission of infrared radiation by the model, which is then used to generate a spectrum that provides information about the chemical bonds in the material; based on the results of the present study, the functional chemical bonds produced by the core-shell (fruit-silica and stem-silica) were similar and showed the presence of the same band peaks in the final product which is an indication for the perfect chemical reaction of the organic components of the Berberis vulgaris extracts and the bioceramic sealer which is similar to the results of a study made by Kazemi poor in Iran (28)

X-ray diffraction (XRD) is commonly used to analyze materials' crystal structure and crystallinity. In the case of silica nanoparticles, XRD can determine if the nanoparticles are crystalline or amorphous and estimate the size of any crystalline regions present (29). The Scherrer equation can estimate the crystallite size, relating FWHM to crystallite size. Assuming a spherical shape, this suggests that the silica nanoparticles are relatively amorphous with some crystallinity. The crystallite sizes for the [101] and [200] peaks are estimated to be 10.6 nm and 10.8 nm, respectively. These values indicate that the nanoparticles have a small crystallite size, consistent with typical silica nanoparticles, which is a critical point to be considered as the size of the nanoparticle is as tiny as possible, as indicated by Nikmah et al. (16), according to the results of the present study the XRD results showed that both SiO$_2$-MPS-Stem extract and SiO$_2$-MPS-fruit extract have amorphous and crystallinity phase.

Several methodologies have been introduced to evaluate the novel core products' structure and size; two of the most common methods are Scanning Electron Microscopy(SEM) and Energy-Dispersive X-ray Spectroscopy (EDX), the SEM of silica nanoparticles showed the spherical shape of the nanoparticles, which is advantageous for many applications as it provides a large surface area to volume ratio, which can enhance reactivity and facilitate surface modification. The well-dispersed nature of the nanoparticles is also essential, as it suggests that

the nanoparticles have good stability in solution and can be easily incorporated into various materials or systems. According to the results of the present study, the ESM and EDX SiO_2-MPS-fruit extract showed that the Preparation of the ceramic-SiO_2-MPS-fruit extract composite resulted in a transformation of the irregular ceramic particles into regular nanospheres with a smaller particle size range(30). The composite material demonstrated a highly uniform and very well-dispersed distribution of particles; EDX analysis confirmed the presence of Zr in the ceramic-SiO_2-MPS-Fruit extract composite, with a higher concentration on the surface. The decrease in Zr weight percentage may be attributed to incorporating SiO_2-MPS-Fruit extract, which can influence the distribution and interaction of Zr atoms in the composite. It is recommended to test the extracts of other plants as well as different plant parts for the synthesis of nanoparticles (31-34).

ESM and EDX analysis of SiO_2-MPS-Stem extract showed that The particle size range of the composite material was reduced to 40-89 nm, suggesting a decrease in particle size compared to the original ceramic particles. This size reduction could be attributed to the additional components present in the composite. Despite the morphological and size changes, the composite material maintained good dispersion, indicating an even distribution of particles without significant agglomeration. In summary, the Preparation of the ceramic-SiO2-MPS-Stem extract composite resulted in the transformation of irregular ceramic particles into quasi-regular nanospheres with a smaller size while preserving good dispersion characteristics.

This novel approach investigated synthesizing a new core-shell structure from nanoparticles enhanced by herbal products from Berberis vulgaris to produce and characterize a novel product that can be used in different medical and dental fields.

In this study, the focus was on improving the mechanical and biological properties of bioceramic mixtures. The active compounds extracted from Berberis vulgaris stems and fruits were analyzed using GC-MS and FTIR, providing insights into their composition. These extracts were then used to synthesize novel nanocomposites, namely SiO2-MPS-stem extract and SiO2-MPS-fruit extract. Characterization techniques such as SEM, EDX mapping, FTIR, and XRD were employed to analyze these composites, confirming the successful coating of silica with the extracts and the formation of core-shell nanostructures with particle sizes below 60 nm. The composites were incorporated into bioceramics for dental root fillings, maintaining an equal weight ratio. The characterized ceramic overlays exhibited nanoscale size, not exceeding 70 nanometers. Notably, the results indicated a core-shell configuration for the nanomaterials, with the shell component consisting of the bioceramic in the case of bioceramic-SiO2-MPS-fruit extract. At the same time, the reverse was observed for bioceramic-SiO2-MPS-stem extract. These findings demonstrate the potential of utilizing bioceramic mixtures enhanced with Berberis vulgaris extracts in dental applications, as they can achieve improved mechanical and biological properties by creating well-defined nanocomposites. Further research and testing are needed to assess their efficacy and safety in dental root-filling procedures.

Consent for publications
The author read and proved the final manuscript for publication.

Availability of data and material
All data generated during this study are included in this published article.

Authors' contribution
All authors had equal roles in study design, work, statistical analysis, and manuscript writing.

Funding

Ethics approval and consent to participate
No humans or animals were used in the present research. The Ethics Committee of Hawler Medical University approved the study protocol.

References

1. Kulinkovych-Levchuk K, Pecci-Lloret MP, Castelo-Baz P, Pecci-Lloret MR, Oñate-Sánchez RE. Guided Endodontics: A Literature Review. Int J Environ Res Public Health. 2022 Oct 26;19(21):13900.

2. Raghavendra SS, Jadhav GR, Gathani KM, Kotadia P. Bioceramics in endodontics - a review. J Istanb Univ Fac Dent. 2017;51(3 Suppl 1):S128–37.

3. Song W, Li S, Tang Q, Chen L, Yuan Z. In vitro biocompatibility and bioactivity of calcium silicate-based bioceramics in endodontics (Review). Int J Mol Med. 2021 Jul;48(1):128.

4. Alsubait S, Albader S, Alajlan N, Alkhunaini N, Niazy A, Almahdy A. Comparison of the antibacterial activity of calcium silicate- and epoxy resin-based endodontic sealers against Enterococcus faecalis biofilms: a confocal laser-scanning microscopy analysis. Odontology. 2019 Oct;107(4):513–20.

5. Karobari MI, Maqbool M, Ahmad P, Abdul MSM, Marya A, Venugopal A, et al. Endodontic Microbiology: A Bibliometric Analysis of the Top 50 Classics. BioMed Res Int. 2021;2021:6657167.

6. Imenshahidi M, Hosseinzadeh H. Berberine and barberry (Berberis vulgaris): A clinical review. Phytother Res PTR. 2019 Mar;33(3):504–23.

7. Arora SS, Shetty R, Hemagiriyappa MS, Thakur SS, Mishra N, Lokhande NM. Comparative Evaluation of Antibacterial Efficacy of Silver and Cadmium Nanoparticles and Calcium Hydroxide against Enterococcus faecalis Biofilm. J Contemp Dent Pract. 2021 Dec 1;22(12):1438–43.

8. Akbarianrad N, Mohammadian F, Alhuyi Nazari M, Rahbani Nobar B. Applications of nanotechnology in endodontic: A Review. Nanomedicine J. 2018 Jul 1;5(3):121–6.

9. Sirkiä SV, Siekkinen M, Qudsia S, Smått JH, Peltonen J, Hupa L, et al. Physicochemical and biological characterization of silica-coated alumina particles. Dent Mater Off Publ Acad Dent Mater. 2022 Dec;38(12):1878–85.

10. Liu X, Wang Z, Zhao C, Bu W, Na H. Preparation and characterization of silane-modified SiO2 particles reinforced resin composites with fluorinated acrylate polymer. J Mech Behav Biomed Mater. 2018 Apr;80:11–9.

11. Rahimzadeh CY, Barzinjy AA, Mohammed AS, Hamad SM. Green synthesis of SiO2 nanoparticles from Rhus coriaria L. extract: Comparison with chemically synthesized SiO2 nanoparticles. PloS One. 2022;17(8):e0268184.

12. Piro NS, Hamad SM, Mohammed AS, Barzinjy AA. Green Synthesis Magnetite (Fe₃O₄) Nanoparticles From Rhus coriaria Extract:

A Characteristic Comparison With a Conventional Chemical Method. IEEE Trans Nanobioscience. 2023 Apr;22(2):308–17.

13. Al-Bermany E, Mekhalif AT, Banimuslem HA, Abdali K, Sabri MM. Effect of green synthesis bimetallic Ag@SiO2 core–shell nanoparticles on absorption behavior and electrical properties of PVA-PEO nanocomposites for optoelectronic applications. Silicon. 2023 Feb 9;1–13.

14. Sabti N, Alalwan H, Alminshid A, Mohammed M. Synthesis and Characterization of Fe3O4- SiO2 Nanoparticles as Adsorbent Material for Methyl Blue Dye Removal from Aqueous Solutions. 2022 Jan 1;

15. Choi M, Choi WK, Jung CH, Kim SB. The surface modification and characterization of SiO2 nanoparticles for higher foam stability. Sci Rep. 2020 Nov 10;10(1):19399.

16. Nikmah A, Taufiq A, Hidayat A. Synthesis and Characterization of Fe 3 O 4 /SiO 2 nanocomposites. IOP Conf Ser Earth Environ Sci. 2019 Jun 3;276:012046.

17. Kim IY, Ohtsuki C, Kamitakahara M, Tanihara M, Cho SB. Effects of polyethylene glycol and methacryloxypropyltrimethoxysilane on morphology and bioactivity of CaO-SiO2 gel prepared by sol-gel method. Key Eng Mater. 2006 Jan 1;309-311 I:317–20.

18. Ning L, Chen J, Sun J, Liu Y, Yi D, Cao J. Preparation and Properties of 3D Printing Light-Curable Resin Modified with Hyperbranched Polysiloxane. ACS Omega. 2021 Sep 9;6(37):23683–90.

19. Zhang J, Lu P, Teng Y, Wang S, Zhang L. In-situ surface modification of precipitated silica nanoparticles with 3-methacryloxypropyltrimethoxysilane in carbonation process. Res Chem Intermed. 2021 Jul 1;47.

20. Nikolic G. Fourier Transforms - New Analytical Approaches and FTIR Strategies [Internet]. 2011 [cited 2023 Jun 2]. Available from: https://www.intechopen.com/books/1574

21. Mohamed MA, Jaafar J, Ismail AF, Othman MHD, Rahman MA. Chapter 1 - Fourier Transform Infrared (FTIR) Spectroscopy. In: Hilal N, Ismail AF, Matsuura T, Oatley-Radcliffe D, editors. Membrane Characterization [Internet]. Elsevier; 2017 [cited 2023 Jun 2]. p. 3–29. Available from: https://www.sciencedirect.com/science/article/pii/B9780444637765000012

22. Alheety NF, Hameed A, Alheety M. Silver Nanoparticles Anchored 5-methoxy benzimidazol thiomethanol (MBITM): Modulate, Characterization and Comparative Studies on MBITM and Ag-MBITM Antibacterial Activities. J Phys Conf Ser. 2019 Oct 25;1294:052026.

23. Segneanu AE, Gozescu I, Dabici A, Sfirloaga P, Szabadai Z, Segneanu AE, et al. Organic Compounds FT-IR Spectroscopy. In: Macro To Nano Spectroscopy [Internet]. IntechOpen; 2012 [cited 2023 Jun 2]. Available from: https://www.intechopen.com/chapters/37659

24. Faramarzi B, Moggio M, Diano N, Portaccio M, Lepore M. A Brief Review of FT-IR Spectroscopy Studies of Sphingolipids in Human Cells. Biophysica. 2023 Mar;3(1):158–80.

25. Yakout SM, Hassan HS. Adsorption Characteristics of Sol Gel-Derived Zirconia for Cesium Ions from Aqueous Solutions. Molecules. 2014 Jul;19(7):9160–72.

26. Matt SB, Raghavendra S, Shivanna M, Sidlinganahalli M, Siddalingappa DM. Electrochemical Detection of Paracetamol by Voltammetry Techniques Using Pure Zirconium Oxide Nanoparticle Based Modified Carbon Paste Electrode. J Inorg Organomet Polym Mater. 2021 Feb;31(2):511–9.

27. Lesbani A, Tamba P, Mohadi R, Fahmariyanti. Preparation of calcium oxide from Achatina fulica as catalyst for production of biodiesel from waste cooking oil. Indones J Chem. 2013 Aug 23;13:176–80.

28. Kazemipoor M, Fadaei Tehrani P, Zandi H, Golvardi Yazdi R. Chemical composition and antibacterial activity of Berberis vulgaris (barberry) against bacteria associated with caries. Clin Exp Dent Res. 2021 Aug;7(4):601–8.

29. Kakuda H, Okada T, Otsuka M, Katsumoto Y, Hasegawa T. Multivariate analysis of DSC-XRD simultaneous measurement data: a study of multistage crystalline structure changes in a linear poly(ethylene imine) thin film. Anal Bioanal Chem. 2009 Jan;393(1):367–76.

30. Najahi-Missaoui W, Arnold RD, Cummings BS. Safe Nanoparticles: Are We There Yet? Int J Mol Sci. 2020 Dec 31;22(1):385.

31. Norani, M., Crawford, A., Aliahmadi, A., Ayyari, M. Evaluation of Tussilago farfara L. Smoke by GC/MS: A Phytochemical Approach to a Traditional Medicine. Agrotech Ind Crops 2023; 3(1): 14-22. doi: 10.22126/atic.2023.8818.1083.

32. Darvishzadeh, R., Khalifani, S. Genetic Variability and Resistance to Orobanche in Oriental Nicotiana tabacum L. Agrotech Ind Crops 2023; 3(1): 30-37. doi: 10.22126/atic.2023.8285.1063.

33. Rostami Ahmadvandi, H., Alavi, S. M., Jabbari, H., Jamshid Moghaddam, M. Quantitative and Qualitative Evaluation of Safflower (Carthamus tinctorius L.) Mutants in Comparison with Commercially Released Cultivars in Iran. Agrotech Ind Crops 2023; 3(1): 38-43. doi: 10.22126/atic.2023.9039.1093.

34. Chaudhary J, Tailor G, Yadav M, Mehta C. Green route synthesis of metallic nanoparticles using various herbal extracts: A review. Biocatal Agric Biotechnol 2023 Apr 8:102692.